Evaluation of the Droplet Collapsibility in Inhalation Drug Delivery through a 3D Computational Study

Ashtiani M. N.[1], Tafazzoli-Shadpour M.[2]*, Najafi H.[3]

[1]Laboratory of Biomechanical Researches, Mechanical Engineering Department, Sahand University of Technology, Tabriz, Iran
[2]Faculty of Biomedical Engineering, Amirkabir University of Technology, Tehran, Iran
[3]Department of Physics, University of Velayat, Iranshahr, Iran

Abstract

Background: Several multiphase flow analyses have been developed to predict the fate of particles used in inhalation drug delivery; however, the collapse of droplets during their passage through respiratory tract has not been investigated.

Objective: To assess the probability of droplet collapse in the upper respiratory tract.

Methods: A 3D model of mouth-to-second generation airway after the trachea was developed with application of a computational fluid dynamics modeling. A new parameter, the droplet collapsibility index (DCI), was defined to evaluate the probability of droplet collapse during the release of droplets through the model.

Results: The results stated that droplets with diameter between 0.1 and 1 μm are at higher risk of collapse. Also, the most probable region of collapse was found to be the glottal bend. The condition becomes progressively worse by increasing the rate of breathing air flow. By increasing the inspiration flow rate from 10 to 30 L/min, the droplet collapsibility rised from 0.75 to 2.25—exceeding the collapsibility threshold.

Conclusion: Results of the current study can be used in evaluation of collapsibility of particles in design of inhalation drug delivery systems.

Keywords

Drug delivery; Respiratory system; Inhalation; Droplet collapsibility; Computational fluid dynamics

Introduction

Inhalation of drug suspended in respiratory air as an aerosol is an efficient, fast and safe method for delivery of pharmaceutics into the human body; this method is also more convenient for the patient [1, 2]. The inhalation drug delivery (IDD) is prescribed for the treatment of many disease conditions including asthma [3, 4], chronic obstructive pulmonary disease [5, 6], cyctic fibrosis [7], lung cancer and lung transplantation disorders [8, 9]. Functional characteristics such as large surface area of the lungs, dense vascularization, thin and highly permeable epithelial layer and proximity of the alveoli to the pulmonary blood capillary beds make the respiratory tract a proper route for drug delivery into the blood circulation [10-13], and consequently into the whole body, the so-called "systemic drug delivery" (SDD) [14]. In this way, many of the neurological disorders, *e.g.*, migraine [15, 16], Alzheimer and Parkinson [17, 18], can effectively employ the IDD for delivery of pharmaceutics. Different studies have been conducted to evaluate the ability of the pulmonary route for delivery of vaccines [19], genes [20],

*Corresponding author: Mohammad Tafazzoli-Shadpour, Faculty of Biomedical Engineering, Amirkabir University of Technology, Tehran, Iran
Tel: +98 21 6454 2385
E-mail: tafazoli@aut.ac.ir

hormones [21], growth factors [22], and some other drugs such as interleukins and heparins [23, 24]. Also, the IDD has been considered as an efficacious delivery option for calcitonin in patients suffering from osteoporosis [25].

Success of a SDD plan depends on several important factors. For instance, the half-life of many newly-synthesized drugs is excessively shorter than the time elapses to reach the targeted area by conventional routes of administration [14], and thus, a faster releasing technique is required. On the other hand, the drug substance in the respiratory tract is more likely to enter the blood circulation without any changes by numerous factors exist in the gastrointestinal tract [26]. Consequently, to satisfy the specifications, the pharmaceutics should be prepared in certain formulations and also released under delimited plans which are closely in relation with the physical features of the drug and its carrier. Such requirements have led to plan for strategies in design of SDD based on drug synthesis methods [27-29] and aerosolization techniques [30-32].

The efficacy of the IDD during breathing is influenced by physical characteristics of the dispersed particles or droplets, *e.g.*, size and shape, density and surface properties [33], and changes in inhalation flow regime which is characterized by inspiration rate, tidal volume and breath holding time [34-36]. In other words, neglecting some physiological reactions such as mucosal clearance [37], one can evaluate the behavior of the therapeutics released into the inspired air using multiphase flow principles. Many of the related computational and experimental studies have focused on analysis of two-phase flow including inhaled air and drug particles [38-40], and the health impact of inhaled toxic particles [41]. Effects of transient and turbulent air flow on particle deposition in the first four airway generations have been evaluated using computational fluid dynamics (CFD) method [42]. Turbulent flow has also been employed to model inhalation in extrathoracic airways (ETAs), disregarding drug as the second phase [43]. In particle deposition, numerical studies have been performed to investigate the effects of transient flow, inlet conditions, out-of-plane angles of the first four bronchi and presence of cartilaginous rings around the trachea on particle deposition and air flow patterns [44, 45]. A numerical study, validated by experiments, showed that the efficiency of the IDD may be improved by optimal combination of particle size, particle release position and inhalation pattern [46]. Furthermore, the role of flow rate and particle size on the deposition of particles in the upper airways has been examined using CFD method [47].

Majority of studies have demonstrated that the physical state of the drug particle, as the second phase dispersed in the air, can be assumed as non-deformable [42, 46-48]. The assumption of rigidity of solid phase is due to negligible viscosity of the air and relatively high modulus of elasticity of particles. However, in situations where the inhaler devices release the liquid pharmaceutics into the respiratory tract, interaction forces between the droplets and the air will become important. Application of unsustainable forces from the environment may lead to collapse of the droplets resulting in failure of the targeted delivery plan, and also overdose in some untargeted areas. Therefore, introducing a new parameter is required to establish the collapsibility of the droplets which has not been investigated in previous studies. On the other hand, various published numerical and experimental analyses related to prediction of the fate of the dry powder particles in respiratory tree estimated that the critical locations of the unwanted early depositions are the ETAs, *i.e.*, mouth-to-throat tract [47]; however, most of these studies have modeled the ETAs separate from the tracheobronchial airways. The objective of this study was therefore to evaluate the intactness of the droplets used in the IDD through an inclusive model of pathways from mouth to the second respiratory airway generations branching after

the trachea. Furthermore, the roles of some effective parameters on collapsibility of the droplets such as droplet size and inspired flow rate were investigated.

Materials and Methods

Theory

Droplet collapse

Fundamentally, a droplet will collapse when all the external forces acting on the surface and volume of the droplet, exceed the resultant internal forces. Therefore, the condition for the initiation of the droplet collapse can be written as:

$$\int_A T \, \mathrm{d}A + \int_V B \, \mathrm{d}V > f_i \qquad (1)$$

where T and B denote tractions and the body forces acting on enclosing surface A and occupying volume V of the droplet, respectively; f_i represents internal forces. By definition, the medium of interest for internal forces has been restricted to the molecules and their interactions. Gravitational body force is negligible at molecular scale. Additionally, since the tractions may be merely originated from the carrier medium, *i.e.*, inspired air, it is rational to institute them using the non-dimensionalized Reynolds number, R_e, describing the ratio of inertial to viscous forces, as expressed as follows:

$$R_e = \frac{\rho u h}{\mu} \qquad (2)$$

where u, ρ, and μ represent surrounding velocity, density and viscosity of the fluid respectively; h is the characteristic length.

On the other hand, the main force which aggregates the molecules of the droplet and resists their separation against external forces is the surface tension that can be represented by Weber dimensionless number, W_e. Such number represents the ratio of inertial forces to the surface tension forces, as follows:

$$W_e = \frac{\rho' v^2 d}{\sigma} \qquad (3)$$

in which ρ is density of the droplet and σ denotes surface tension coefficient. Parameters v and d denote droplet velocity and diameter, respectively. By elimination of the inertial forces between R_e and W_e, the remaining ratio appears as a practical index for identification of the collapse of the droplet. The deduced droplet collapsibility index (DCI) will be finally obtained as:

$$DCI = \frac{\rho' \mu}{\rho \sigma} \frac{v^2}{u} \frac{d}{h} \qquad (4)$$

Such parameter becomes influential when the density ratio is quite large. The value of the DCI as a function of anatomical location in the ETAs and the early generations is developed.

Turbulent flow

The turbulent nature of the inspired air flow in the respiratory tract has been simulated by Renormalization Group k-e (RNG k-ε) model which is based on instantaneous solving of Navier-Stokes equations and can be introduced by two transport equations [43]:

$$\frac{\partial}{\partial x_i}(\rho u_i k) = \frac{\partial}{\partial x_i}\left(\alpha_k \mu_{eff} \frac{\partial k}{\partial x_i}\right) + G_k + S_k - \rho\varepsilon, \qquad (5)$$

$$\frac{\partial}{\partial x_i}(\rho u_i \varepsilon) = \frac{\partial}{\partial x_i}\left(\alpha_k \mu_{eff} \frac{\partial k}{\partial x_i}\right) + C_1 \frac{\varepsilon}{k} G_k - C_2 \rho \frac{\varepsilon^2}{k} + S_k - R_\varepsilon \qquad (6)$$

The above equations relate two terms of the turbulent kinetic energy, k, and energy dissipation rate, ε. Parameters u, ρ and x_i represent the velocity, density and position vector, respectively. The effective turbulent viscosity of the fluid, μ_{eff}, has been correlated to the laminar viscosity, μ, as:

$$d\left(\frac{\rho^2 \kappa}{\sqrt{\varepsilon \mu}}\right) = 1.72 \frac{\hat{\nu}}{\sqrt{\hat{\nu}^3 - 1 + C_\nu}} d\hat{\nu} \qquad (7)$$

where

$$\hat{v} = \frac{\mu_{eff}}{\mu} \quad (8)$$

and $C_n = 100$. Moreover, α_k represents the inversed effective Prandtl number for turbulent kinetic energy, G_k is the generation of turbulence energy due to the mean velocity gradients, and S_k is the source of energy produced. The parameter R_e can be derived by the following equation [43]:

$$R_\varepsilon = \frac{C_\mu \rho v^3 \left(1 - v / v_0\right)}{1 + \beta v^3} \frac{\varepsilon^2}{\kappa} \quad (9)$$

where

$$v \equiv \frac{S_\kappa}{\varepsilon} \quad (10)$$

and $v_0 = 4.38$, $b = 0.012$ and $C_m = 0.0845$. Additionally, C_1 and C_2 in the two main equations are respectively, equal to 1.24 and 1.68, based on analytical methods [43].

Modeling

Geometry

Complex geometry of the upper airways causes unusual flow patterns in this region [43]. In addition to the enhanced probability of the droplet collapsibility, this may alter the commonly considered inlet conditions for the trachea. Therefore, it is important to simulate an inclusive model of the ETAs and the first three generations. The model contains the oral cavity, the larynx, the pharynx, the glottis, the trachea and the first and second generation bronchi (Fig. 1). Knowing what will happen within the following generations can be satisfactorily deduced by such analytical interpretations. The geometry is asymmetric in the sagittal plane, but the out-of-plane orientations of the bronchi in the coronal plane have been disregarded [39]. The tracheal cartilaginous rings have been included, as their contribution to the flow regime has already been suggested [49].

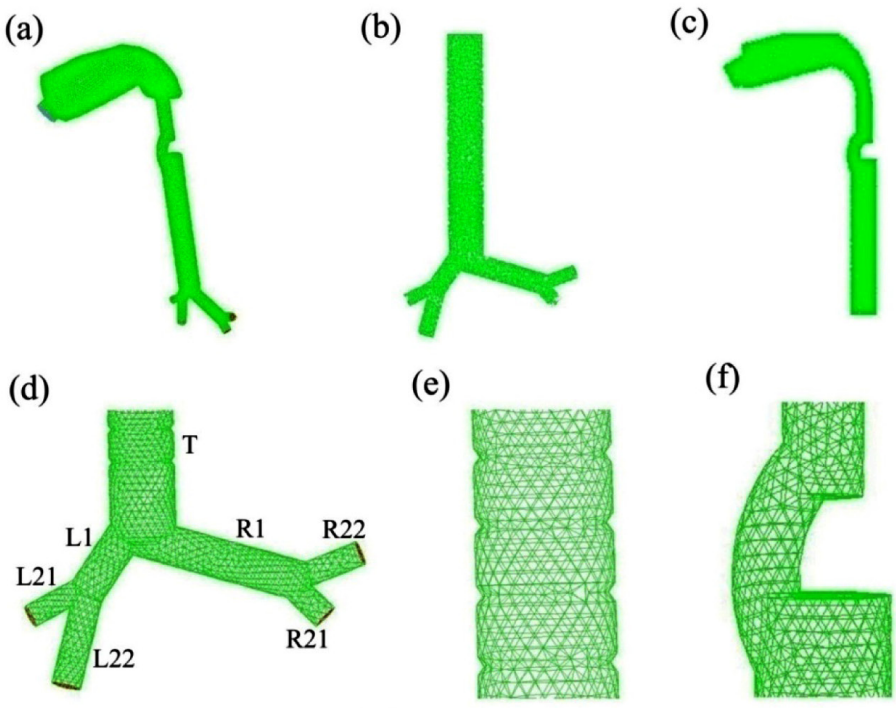

Figure 1: Three-dimensional model of mouth-to-second generation airways; (a) the 3D model, (b) coronal section of the intrathoracic part of the model, (c) sagittal section of the extrathoracic part of the model, (d) magnification of branches, (e) magnification of tracheal cartilaginous rings, and (f) magnification of the glottal bend

Table 1: Geometrical characteristics of the intrathoracic part of the model. In the labels, T stands for trachea, R for right and L for left branches. Also, the first number after the letter denotes the generation number.

Generation number	Figure label	Diameter (mm)	Length (mm)	Orientation angle (degree)
0	T	18	125	0
1	L1	11	22	35
1	R1	12	50	73
2	L21	7.3	15.6	63
2	L22	9	26	15
2	R21	8	11	44
2	R22	7.5	16	48

The geometric data of the ETAs used in the model are averaged dimensions of human upper airways, and those are associated with bronchial tree represented in Table 1, based on asymmetric model of the human lung developed previously [50]. The structural meshing of the model has been developed using 17,555 nodes and 82,519 quadrilateral elements. Based on the aforementioned constitutive equations, the generated model has been analyzed through computational fluid dynamics method utilizing commercial software FLUENT version 6.3.

Boundary conditions and loading

All the lateral walls have been assigned by no slip boundary condition for the fluid, and the inlet of the tract has been assumed to be under the velocity-inlet condition valued in accordance with those listed in Table 2, for normal and deep breathing flow rates [43].

The analysis included two phases of carrier medium and drug droplets. The carrier medium was assumed to be natural air at 25 °C with negligible effect of temperature on the density [43]. Since the maximum value of the non-dimensionalized Mach number for fluid does not exceed 0.3 [45], we assumed that the inspired air was incompressible.

Material properties

The laminar density and viscosity of the atmospheric air (described in Eq. 7) were assumed to be 1.225 kg/m^3 and 1.8×10^{-5} kg/m.s, respectively [43]. For the second phase of the mixture, *i.e.*, the droplets, the physical properties of the water were considered [6]; therefore, the values of 998 kg/m^3 and 0.001 kg/m.s were set for density and viscosity [48, 49]. The shape of the droplets was also assumed to be spherical [31, 49]. The size of the droplet was assumed to vary from 0.1 to 100 μm, as one of the variables in the study.

Solution criterion of the multiphase flow analysis was based on the Eulerian model which solves the continuity and momentum equations for each phase separately and then the coupling is performed by coupling the pressure values between the phases.

Results

The parameter DCI was defined to designate the power of the viscous forces, acting by the

Table 2: Velocity inlet magnitudes for two flow rates

Flow rate (L/min)	Velocity (m/s)
10	0.53
30	1.59

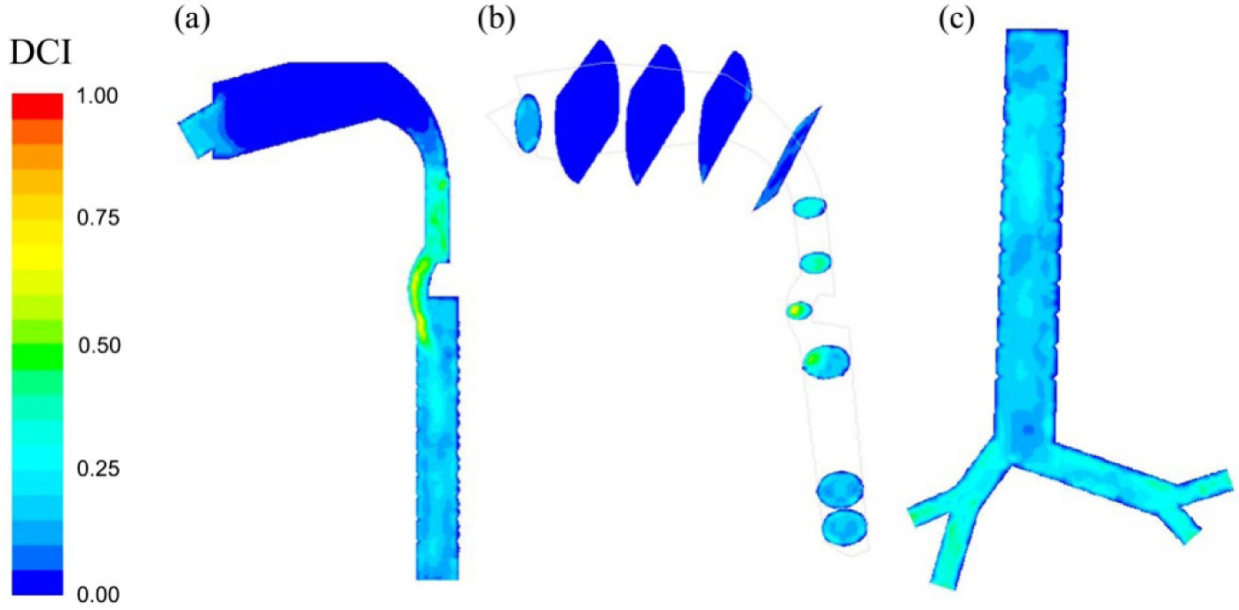

Figure 2: Contours of the DCI for (a) sagittal section of the extrathoracic part of the model, (b) serial cross-sections normal to the pathway, and (c) coronal section of intrathoracic part of the model

carrier medium on the droplet surface, against the surface tension forces. Noticeably, the DCI depends on the fluid mechanical features of the airways which are variable from one anatomical location to another. Therefore, it gained different values along the model. Figure 2 shows how the DCI varies along anatomical sites in sagittal and coronal sections of the model, for the droplets of 1 μm in diameter and the an airflow rate of 10 L/min.

Variation in size of droplets dispersed in the inspired air can alter the distribution pattern and magnitude of the DCI. Figure 3 illustrates how alteration in the size influences the intactness of the droplets during their passages through the airways. Results are presented for different anatomical regions including oral cavity, the pharynx, the larynx and the glottis, superior part of the trachea, inferior part of the trachea, and the first and second generation airways. The value of DCI was developed for four logarithmic sizes from 0.1 to 100 μm.

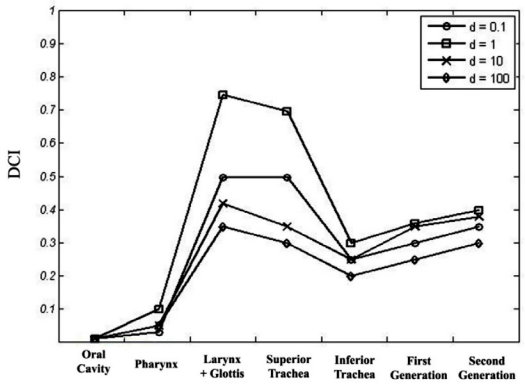

Figure 3: Average regional values of the DCI for four droplet sizes (μm)

Any alteration in the airflow rate may result in variation of breathing pattern which consequently influences the behavior of the drug droplets. The diagram of Figure 4 indicates a noticeable rise in the value of the DCI once air is inspired by two flow rates of 10 and 30 L/min. Besides the overall increase in the amount of DCI for higher flow rates, variations in the DCI were also greater among the anatomical sites. The graph of the 30 L/min inspiration rate describes that DCI exceeds the collapse threshold (unit DCI) at the end of the pharynx. However, the maximum DCI occurred at the superior part of the trachea by a magnitude of approximately 2.25. In accordance with the diagram of Figure 4, the contours of the DCI in the ETAs are demonstrated in Figure 5 indicating that at higher flow rates, the mouth

is still remained safe against the collapsibility of droplets. However, the risk area is extended upward to the pharynx.

Discussion

Using CFD method, the collapsibility of the droplet drugs was analyzed through the human respiratory tract by introducing a droplet collapsibility index. Moreover, effects of the deep breathing (represented by increased airflow rate) and changes in the droplet size on the collapse of the droplets were investigated.

Since the DCI represents the balance of the viscous and surface tension forces around and inside the droplet, the value of DCI equal to 1, is considered as the collapsibility threshold, *i.e.*, once it exceeds this value, the external viscous forces becomes greater and the droplet collapses. Under normal breathing condition and droplets with 1 µm in diameter, the maximum value of the DCI is approximately 0.75

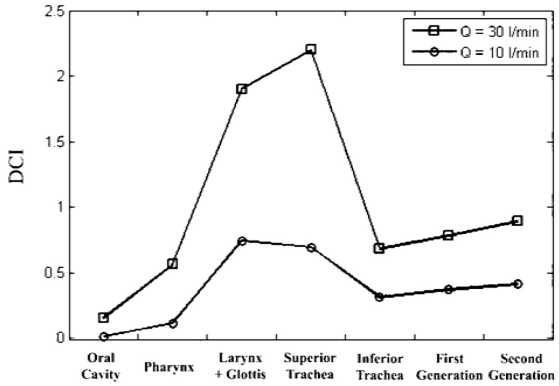

Figure 4: Average regional values of the DCI for two droplet sizes and two typical flow rates

occurred at the glottal bend. As the velocity of the carrier phase is of moderate magnitude, the internal surface tension forces exist between the molecules of the droplet can tolerate the viscous forces and the DCI is lower than 0.5 in most of the anatomical locations. However, exceptionally at the glottal bend, the velocity

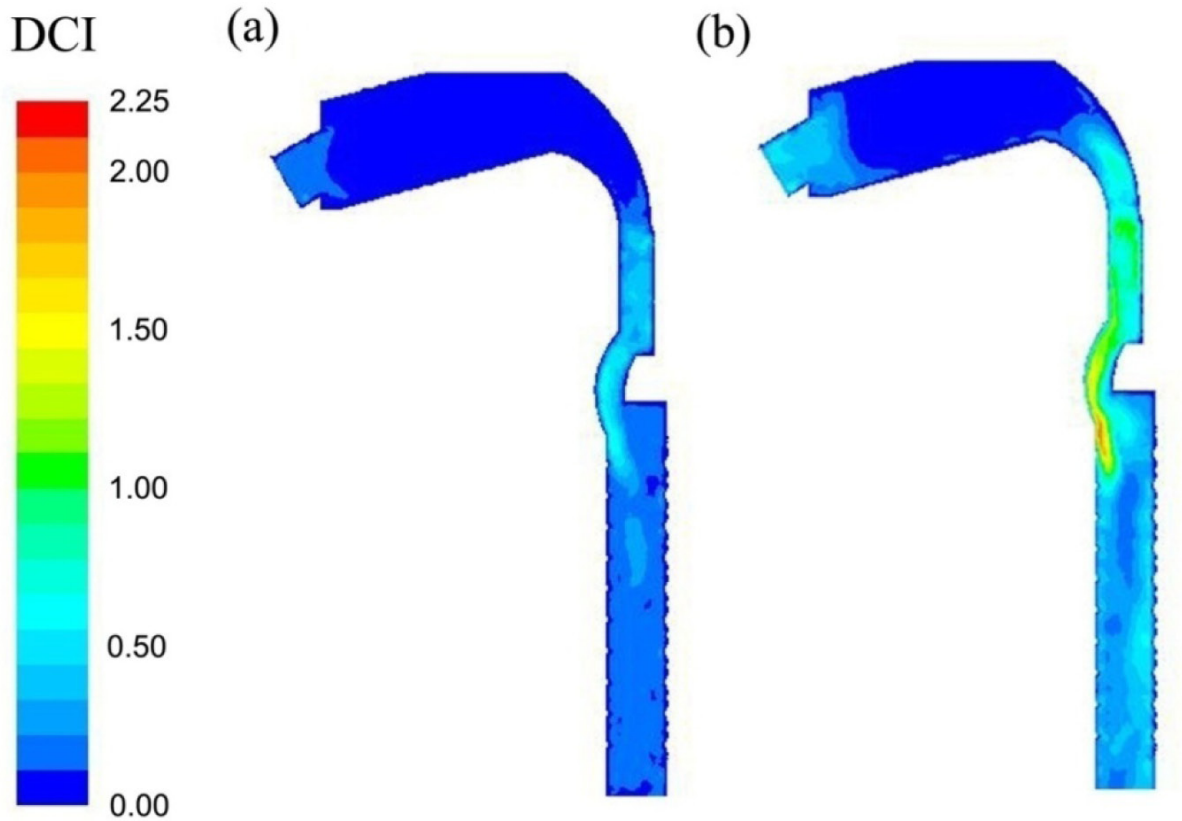

Figure 5: Contours of the DCI in sagittal section of 1 µm-sized droplets for (a) Q = 10 L/min, and (b) Q = 30 L/min

increases considerably due to reduction in the sectional area. Roughly, all the previous investigations with multiphase modeling of the IDD reported the maximum velocity at the glottal bend [39, 46, 47]. Moreover, the curvature of the glottis violates the uniformity of the velocity vectors across the section (Fig. 2b), leading to generation of adverse vortices at the following regions. This may move a considerable percentage of the droplets to the anterior wall of the trachea and hinder or even trap the rest and finally collapse them. This phenomenon has also been mentioned in other studies [46]. Results showed that early-branched intrathoracic airways of the pulmonary tree gain higher values of the DCI in comparison with the inferior trachea because of relatively higher air velocities in that region; this finding is compatible with results of other numerical studies [39, 46]. Nevertheless, sequential branching of the generations reduces the percentage of the flow entering each of them. As shown in Figure 3, after a noticeable fall through the trachea, there is a slow rise in the DCI starts; however, due to the enormous number of the branches deep inside the lung, the share of the airflow rate and consequently the air velocity decreases significantly. Such reduction in the velocity is notably more prominent than that of diameter (characteristic length) of bronchioles. With a preliminary assessment, the DCI for the trachea is roughly 19.5 times greater than that for the alveolar ducts. This is why, viscous forces become remarkably weaker than surface tension, and therefore, it is predicted that the probability of a droplet collapse decreases.

When different diameters of 0.1, 1, 10 and 100 μm were taken into account, results showed a non-linear behavior. Among different diameters, lowest values of the DCI occurred in droplets with largest diameters. In other words, droplets with 10 μm diameter followed the pattern of the 100 μm-sized ones except with slightly more magnitudes of DCI. Fundamentally, dispersion of the larger droplets in the respiratory air decreases the turbulence intensity and then the average velocity of the mixture; therefore, the viscous forces are remained weaker than the surface tensions. However, the results of droplets 0.1 μm in diameter stated that the collapsibility is not directly related to the droplet size 1 μm droplets were of higher risk of collapse (Fig. 3) due to the mutual effects of the velocity changes and diameter on the surface tension forces.

The possibility of the collapse of droplets was strongly influenced by the inlet conditions. Clearly, once the patient deeply inhales the air mixed with the drug droplets, *i.e.*, when the flow rate increases, a dramatic rise in the viscous forces is generated around the droplet. In this way, by a three times deeper inspiration, the DCI is elevated up to 2.2—implying that the viscous forces excessively surpass the internal tension forces. Another important difference observed in 30 L/min air flow rate was that the site of maximal DCI moves forward to the superior part of the trachea instead of the larynx and the glottal bend. This alteration is due to effects of the increased turbulence intensity as previously described [39, 47], anatomical curvature of the glottis, and higher velocities. In other words, higher viscous forces act on the droplets when they gain maximum velocities at the end of the glottis entering the trachea, although the main rise (approximately from 0.5 to 1.9) in the DCI is still due to the sectional area reduction in the glottal bend. This is also shown in Figure 5 for 1 μm droplets under 10 and 30 L/min air flow rates.

In conclusion, it was shown that under normal breathing conditions, the droplets with 0.1 to 1 μm in diameter are at higher risk of collapse, remarkably at glottal bend. Also, deep inhalations immoderately menace the intactness of droplets and spread the probable areas of collapsibility from glottal bend to the superior regions of trachea. Therefore, if the target of the IDD is the intrathoracic airways or the alveoli, the liquid carriers, specifically

between 0.1 and 1 μm, may collapse while passing through the ETAs and overdose these areas.

References

1. Hickey AJ, Thompson DC. Physiology of the airways. In: Hickey AJ, editor. *Pharmaceutical inhalation aerosol technology*. 2nd ed. New York: Marcel Dekker; **2004**;1.
2. Choi WS, Krishna Murthy GG, Edwards DA, *et al.* Inhalation delivery of proteins from ethanol suspensions. *Proc Natl Acad Sci USA* 2001;**98**:11103-7.
3. Smyth H. Exipients for pulmonary formulations. In: Katdare A, Chaubal MV, editors. *Exipients development for pharmaceutical, biotechnology and drug delivery systems.* New York: Informa Health Care USA; **2006;**225.
4. Dalby R, Suman J. Inhalation therapy: technological milestones in asthma treatment. *Adv Drug Deliv Rev* 2003;**55**:779-91.
5. Segal RA, Martonen TB, Kim CS, Shearer M. Computer simulation of particle deposition in the lungs of chronic obstructive pulmonary disease patients. *Inhal Toxicol* 2002;**14**:705-20.
6. Ali M. The Pulmonary Drug Delivery.In: Kulkarni V, editor. *Minimally invasive drug delivery systems*. Norwich, NY: WilliamAndrew Inc.; **2009;**218.
7. Green JD. Pharmaco-toxicological expert report PulmozymerhDNase Genentech. Inc. *Hum Exp-Toxicol* 1994;**13**:S1-S42.
8. Wauthoz N, Deleuze P, Hecq J, *et al.* In vivo assessment of temozolomide local delivery for lung cancer inhalation therapy. *Eur J Pharm Sci* 2010;**39**(5):402-11.
9. Corcoran TE. Inhaled delivery of aerosolized cyclosporine. *Adv Drug Deliv Rev* 2006;**58**:1119-27.
10. Scheuch G, Kohlhaeufl MJ, Brand P, Siekmeier R. Clinical perspectives on pulmonary systemic and macromolecular delivery. *Adv Drug Deliv Rev* 2006;**58**:996-1008.
11. Patton JS, Platz RM. Routes of delivery: case studies: (2) pulmonary delivery of peptides and proteins for systemic action. *Adv Drug Deliv Rev* 1992;**8**:179-96.
12. Niven RW. Delivery of biotherapeutics by inhalation aerosol. *Crit Rev Ther Drug Carrier Syst* 1995;**12**:151-231.
13. Finlay WH. *The mechanics of inhaled pharmaceutical aerosols*. San Diego: Academic Press; **2001**.
14. Saltzman WM. *Drug delivery: engineering principles for drug therapy*. New York: Oxford University Press; **2001**.
15. Silberstein SD. Meeting acute migraine treatment needs through novel treatment formulations. *Neurotherapeutics* 2010;**7**:153-8.
16. Illum L. Nasal drug delivery: developments and strategies. *Drug Deliv Today* 2002;**7**:1184-9.
17. Minn A, Leclerc S, Heydel JM, Minn AL, *et al.* Drug transport into the mammalian brain: the nasal pathway and its specific metabolic barrier. *J Drug Target* 2002;**10**(4):185-96.
18. Goole J, Amidi K. Levodopa delivery systems for the treatment of Parkinson's disease: an overview. *Int J Pharm* 2009;**380**:1-15.
19. LiCalsi C, Christensen T, Bennett JV, *et al.* Dry powder inhalation as a potential delivery method for vaccines. *Vaccine* 1999;**17**:1796-803.
20. Sanders N, Rudolph C, Braeckmans K, *et al.* Extracellular barriers in respiratory gene therapy. *Adv Drug Deliv Rev* 2009;**61**:115-27.
21. Bosquillon C, Preat V, Vanbever R. Pulmonary delivery of growth hormone using dry powders and visualization of its local fate in rats. *J Control Release* 2004;**96**:233-44.
22. Edwards DA, Ben-Jebria A, Langer R. Recent advances in pulmonary drug delivery using large, porous inhaled particles. *J Appl Physiol* 1998;**85**:379-85.
23. Qi Y, Zhao G, Liu D, *et al.* Delivery of therapeutic levels of heparin and low-molecular-weight heparin through a pulmonary route. *Proc Natl Acad Sci USA* 2004;**101**:9867-72.
24. Yue T, Jia-bi Z. Recombinant human interleukin-2 inhalation powders: preparation and distribution in the alveolus. *Int J Pharm* 2008;**360**:225-7.
25. Patton JS. Pulmonary delivery of drugs for bone disorders. *Adv Drug Deliv Rev* 2000;**42**:239-48.
26. Burke PA. Controlled release protein therapeutics: effects of process and formulation on stability. In: Wise DL, ed. *Handbook of pharmaceutical controlled release technology*. New York: Marcel Dekker; **2000**;661-92.
27. Pison U, Welte T, Giersig M, Groneberg DA. Nanomedicine for respiratory diseases. *Eur J Pharmacol* 2006;**533**:341-50.
28. Amidi M, Krudys KM, Snel CJ, *et al.* Efficacy of pulmonary insulin delivery in diabetic rats: Use of a model-based approach in the evaluation of insulin powder formulations. *J Control Release* 2008;**127**:257-66.
29. Khatri K, Goyal AK, Gupta PN, *et al.* Surface

modified liposomes for nasal delivery of DNA vaccine. *Vaccine* 2008;**26**:2225-33.

30. Leong KH. Theoretical principles and devices used to generate aerosols for research. In: *Hickey AJ, editor. Pharmaceutical inhalation aerosol technology*. New York: Marcel Dekker; **2004;**254.
31. Atkins PJ, Crowder TM. The design and development of inhalation drug delivery systems. In: Hickey AJ, editor. *Pharmaceutical inhalation aerosol technology*. New York: Marcel Dekker; **2004;**287.
32. Minne A, Boireau H, Joao Horta M, Vanbever R. Optimization of the aerosolization properties of an inhalation dry powder based on selection of excipients. *Eur J Pharm Biopharm* 2008;**70**:839-44.
33. Vincent JH, Johnston AM, Jones AD, *et al.* Kinetics of deposition and clearance of inhaled mineral dusts during chronic exposure. *Br J Ind Med* 1985;**42**:707-15.
34. Newman SP, Pavia D, Garland N, Clarke SW. Effects of various inhalation modes on the deposition of radioactive pressurized aerosols. *Eur J Respir Dis Suppl* 1982;**119**:57-65.
35. Martonen TB, Katz IM. Deposition patterns of aerosolized drugs within human lungs-effects of ventilatory parameters. *Pharm Res* 1993;**10**:871-8.
36. Byron PR, Patton JS. Drug delivery via the respiratory tract. *J Aerosol Med* 1994;**7**:49-75.
37. Knowles MR, Boucher RC. Mucus clearance as a primary innate defense mechanism for mammalian airways. *J Clin Invest* 2002;**109**:571-7.
38. Zhang Z, Kleinstreuer C. Transient airflow structures and particle transport in a sequentially branching lung airway model. *Phys Fluids* 2002;**14**:862-80.
39. Zhang Z, Kleinstreuer C. Airflow structures and nano-particle deposition in a human upper airway model. *J Comput Phys* 2004;**198**:178-210.
40. Gonda I. Particle deposition in the human respiratory tract. In: Crystal RG, West JB, Weibel ER, Barnes PJ, ed. *The lung: scientific foundations.* Philadelphia: Lippincott-Raven Publishers; **1997;** 2289.
41. Pope CA, Dockery DW, Schwartz J. Review of epidemiological evidence of health effects of particulate air pollution. *Inhal Toxicol* 1995;**7**:1-18.
42. Worth-Longest P, Vinchurkar S. Validating CFD predictions of respiratory aerosol deposition: effects of upstream transition and turbulence. *J Biomech* 2007;**40**:305-16.
43. Ball CG, Uddin M, Pollard A. High resolution turbulence modeling of airflow in an idealized human extra-thoracic airway. *Comput Fluids* 2008;**37**:943-64.
44. Li Z, Kleinstreuer C, Zhang Z. Simulation of airflow fields and microparticle deposition in realistic human lung airway models. Part I: airflow pattern. *Euro J of Mech B/Fluids* 2007;**26**:632-49.
45. Li Z, Kleinstreuer C, Zhang Z. Simulation of airflow fields and microparticle deposition in realistic human lung airway models. Part II: particle transport and deposition. *Euro J of Mech B/Fluids* 2007;**26**:650-68.
46. Kleinstreuer C, Zhang Z, Zhang L, *et al.* A new methodology for targeting drug-aerosols in the human respiratory system. *Int J Heat Mass Transfer* 2008;**51**:5578-89.
47. Jayaraju ST, Brouns M, Verbanck S, Lacor C. Fluid flow and particle deposition analysis in a realistic extrathoracic airway model using unstructured grids. *J Aerosol Sci* 2007;**38**:494-508.
48. Li Z, Kleinstreuer C, Zhang Z. Particle deposition in the human tracheobronchial airways due to transient inspiratory flow patterns. *J Aerosol Sci* 2007;**38**:625-44.
49. Russo J, Robinson R, Oldham MJ. Effects of cartilage rings on airflow and particle deposition in the trachea and main bronchi. *J Med Eng Phys* 2008;**30**:581-9.
50. Horsfield K, Dart G, Olson DE. Models of human bronchial tree. *J Appl Physiol* 1971;**31**:207-17.